



Special Feature: Nano Structured Devices

Research Report

Signal Detection with Nanomechanical Systems and Its Improvement by Utilizing Noise

Yukihiro Tadokoro, Hiroya Tanaka, Keita Funayama and Yutaka Ohno

Report received on Jun. 27, 2019

■ABSTRACT■ In this study, a nanoscale phase detector that can digitally receive and detect phase-modulated signals is proposed. The mechanical vibration of a tip of carbon nanotube, which is controlled by an electromagnetic field from a metal plate, realizes two key functions for communications: reception and detection of signals at the nanoscale. Indeed, our theoretical analysis shows the possibility of detection; however, because of the nanoscale reception, the received signal power is strongly reduced. To solve this problem, a counter-method of the current enhancement is introduced in which the time averaging of the noisy field emission current served to amplify the received signal. The numerical results and the foundational theory describing the mechanism of the enhancement demonstrate the effectiveness of the proposed method.

■KEYWORDS■ Nanomechanical Systems, Carbon Nanotube, Phase Detector, Stochastic Resonance, Noise-enhanced System

1. Introduction

Sensing and communication with ultra-small devices should contribute to the future-promising applications and services.⁽¹⁾ For example, smart dust^(2,3) can detect various quantities such as temperature, light, and vibrations with invisible sensor nodes. However, after the data is collected, communication among nodes and/or a central station is crucial for delivering and analyzing the collected data. Nano-sensor networks have been proposed to realize this level of communication. Communication between physically separated nodes could be achieved by using electromagnetic (EM) waves as information carriers.^(4,5)

Signal processing algorithms for communications are typically implemented on micro-scale complementary metal-oxide semiconductor (CMOS)-based chips. However, the analog and radio frequency (RF) components require too much space in the node to allow for miniaturization. For instance, since design process for EM-based antennas follows electromagnetic framework, the antenna size is on the order of the signal wavelength.⁽⁶⁾ The megahertz band is often focused due to the advantage for signal propagation; in this case, the antenna size must not be less than several centimeters, resulting in a large node.

To solve this problem, leading studies have tried to use the terahertz region,⁽⁷⁻⁹⁾ which allows the antenna size to be considerably reduced (as small as 1 μm), thus realizing the miniaturization. However, designs of the circuits and signal source for such ultra-high frequencies are quite complicated.

A method for sensing and communications for the miniaturization has been addressed by exploiting the nano-mechanical resonator (NMR). Mechanical vibration can describe physical quantities, which can be detected in nanoscale.⁽¹⁰⁻¹²⁾ Some proposed sensing applications include chemical sensors,^(13,14) temperature sensors,⁽¹⁵⁾ and mass sensors.^(16,17) The dynamics of carbon nanotubes (CNTs), which are key materials in these applications, have been well investigated,⁽¹⁸⁻²⁰⁾ and a large responses for weak signals by exploiting mechanical resonance has been demonstrated.^(12,17) A pioneering work by Jensen et al. shows an NMR-based nanoantenna for a FM radio receiver.⁽²¹⁾ This interesting concept has been extended in other studies.^(5,22) Operating in the megahertz band was addressed with an antenna element in nanoscale. Tanaka et al. have discussed the angular sensitivity, which is one of the most important characteristics in antenna systems,⁽²³⁾ and have presented a design method for this concept.⁽²⁴⁾ However, these antennas cannot detect the digitally

phase-modulated signals, which are often focused in recent communication systems. As shown in Sec. 3. 2. 2, the output of these nanoantennas varies with a rate of the twice of the carrier frequency. Owing to this nonlinear behavior, the output of nanoantennas is not effective to detect phase-modulated signals.

The nanomechanical system examined in this study contributes to the development of nanoscale receivers, particularly, the demodulator/detector and receiver antenna. Against previous studies, digital communication with phase-modulated signals is focused in this study. Two important functions are realized at nanoscale via mechanical vibration of a CNT tip: reception of the incoming signal in the megahertz band and detection of the carrier phase that describes the transmitted data. The proposed method realizes these functions by the simple introduction of a reference EM wave coming from the metal plate placed below the CNT. The reference wave induces static and oscillating EM fields. The oscillating field enables to describe the carrier phase on the vibration amplitude, whereas the static field breaks the symmetry of the CNT motion, giving rise to a component related to the vibration at the resonance frequency. The signal phase is detected by measuring the amplitude of this component. Our theoretical analysis reveals that, due to the biased reference EM wave, two frequency components are included in the current. Exploiting this interesting characteristic, the transmitted data is detected via the demodulator, which focuses on the two frequency components.

To ensure the reliable communication on the proposed detector, a sufficiently strong current is required, which in turn requires to apply a large voltage between the electrodes. The production of such a large voltage, however, needs a strong power source. In the development of the nanoscale systems and devices, this is often a bottleneck. In this study, a method is proposed with exploiting the surrounding noise. In nonlinear physics, interesting phenomenon of Stochastic resonance (SR) has been discussed, in which noise has a constructive role in signal detection. The proposed method in this study is based on this framework.⁽²⁵⁻²⁷⁾ In the proposed method, a noise component contained in the current is used to amplify the current. However, simply exploiting noise is not sufficient to obtain the amplification. We introduce an additional step in signal-processing: time-averaging of the noisy current. Our theoretical analysis shows

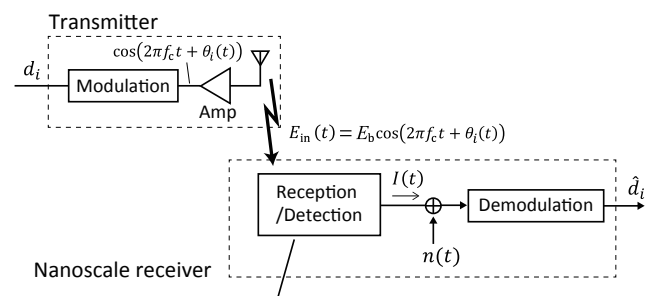
that by modulating the probability density of the noisy current, the amplification is obtained. Such enhancement effect can be realized in any systems with nonlinear behavior, and the resulting field emission current shows nonlinear, specifically exponential behavior.

2. System Model

The simple system proposed in this study contained a transmitter for sending the modulated signal for digital data signal $d_i \in \{+1, -1\}$ to a receiver. The signal was detected at the receiver using the proposed nanoscale phase detector, and the transmitted data was estimated in the demodulator. **Figure 1** depicts the system diagram.

Each data bit d_i was mapped to the corresponding phase of the carrier signal in the transmitter. For the simple discussion, binary phase-shift keying (BPSK) modulation was employed, and the digital data were encoded on the phase with the following rule: $\theta_i = \theta_0 + \pi$ for $d_i = +1$ and $\theta_i = \theta_0$ for $d_i = -1$. Here, we consider a phase offset θ_0 between the transmitter and the receiver. The modulated signal with frequency f_c was expressed as $\cos(2\pi f_c t + \theta_i)$ with the phase signal $\theta_i(t)$ defined as $\theta_i = \sum_{i=-\infty}^{+\infty} \theta_i g_{T_b}(t - T_b)$, where $g_{T_b}(t) = +1$ for $0 \leq t \leq \tau$ and $g_{T_b}(t) = 0$ for the other time-region, i.e., $t < 0$ and $t > \tau$, with the bit duration T_b . Finally, the carrier signal $E_{in}(t)$ with amplitude E_b was received at the receiver.

At the front end of the receiver, the proposed nanoscale phase detector, provided in Sec. 3, was installed. The incoming signal was detected through



The proposed nanoscale phase detector (Fig. 2(a)) is employed.

Fig. 1 Communication system with the proposed nanoscale phase detector.

mechanical vibration of the CNT, and the detector output was the field emission current that described the phase information of the incoming signal. Key functions in the detection of phase-modulated signals, such as frequency tuning, signal reception, and phase detection, could be realized in a single nanoscale structure. The demodulator is discussed in Sec. 4 in which a correlator was employed to calculate the correlation between the current and the carrier signal. The transmitted data was finally estimated by making hard decision to the correlation.

3. Nanoscale Phase Detection Based on the Mechanical Vibration of CNT

3.1. Nanoscale Phase Detection Concept

Along with previously developed nanoantenna system, the nanoscale phase detector is introduced.⁽²¹⁾ The structure of the proposed detector is given in Fig. 2(a), where h_0 is the distance between the tip of the CNT and the anode when the tip is in the equilibrium position (point o) and $h(t)$ is the distance at a time t ; this gives $\Delta h(t) = h(t) - h_0$.

First, the mechanism of the original nanoantenna system⁽²¹⁾ can be described briefly as follows. The application of external voltage V_{ext} causes a charge to be excited around the tip of the CNT. When the signal (EM wave) arrives at the CNT, Coulomb's law

states that an electrostatic force is applied at the tip. This force is the source of the vibration of the tip; for example, when the signal $E_{\text{in}}(t)$ is positive, the signal attracts the tip, i.e., the tip moves in the direction of signal propagation (positive x direction in Fig.2(a)). Because of the EM interaction between the incoming signal and the charge, vibration can be used to detect the phase and the amplitude of the incoming signal. If the frequency of the incoming signal matches the mechanical resonance frequency of the CNT, the vibration amplitude is strongly enhanced. This means that "frequency tuning" can be performed, which contributes to the nanoscale signal reception. The vibration is observed using the field emission current, which means that the detector receives the incoming signal through the current. However, as discussed in Ref. (22), this method has low reception sensitivity because of the small device size.

As discussed at the end of Sec. 3. 2. 2, the original system⁽²¹⁾ cannot receive phase-modulated signals. However, in the proposed detector, the phase of phase-modulated signals could be obtained if a metal plate was placed below the CNT and a sinusoidal reference voltage $V_{\text{ref}}(t)$ was applied with frequency f_c . In the proposed setup, the tip was exposed to an EM field with a magnitude of $E_{\text{ref}}(t) = \tilde{E}_{\text{ref}} \cos(2\pi f_c t) + \bar{E}_{\text{ref}}$, causing a force to arise between the plate and the tip. The applied force combined with the incoming and reference signals

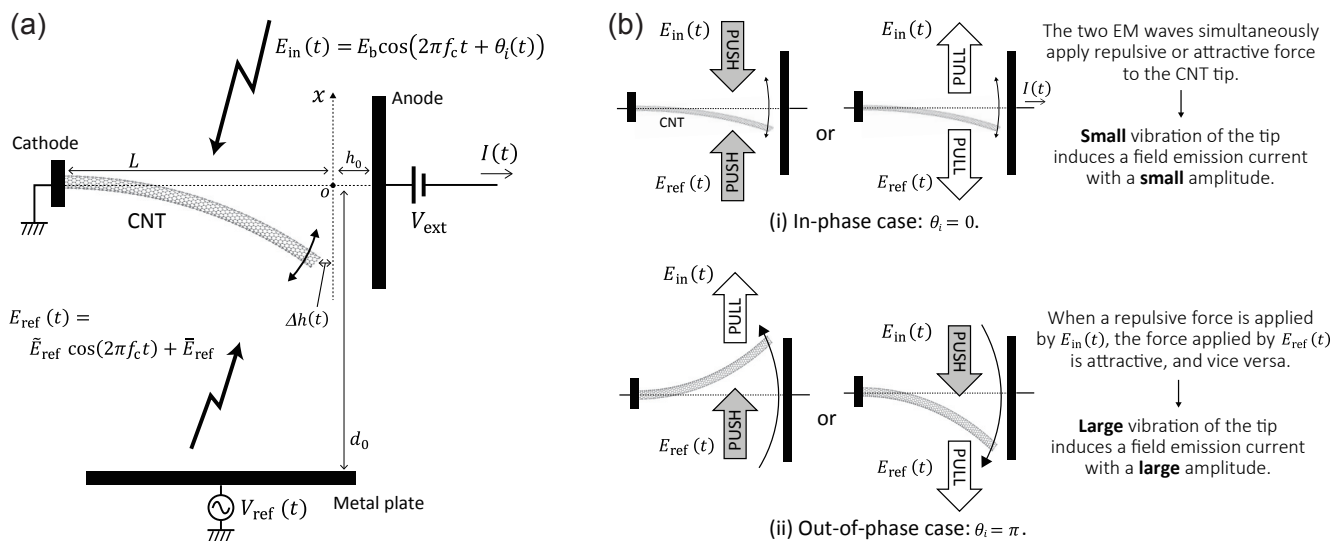


Fig. 2 (a) Structure of the proposed nanoscale phase detector. (b) Illustrative sketch of the mechanism of the detector.

caused the CNT top to vibrate. The magnitude of the combined force depended on the phase (see Eq. (3)). An illustrative sketch of the mechanism is provided in Fig. 2(b). For example, in the in-phase case, because the tip received either an attractive or a repulsive force from the signals, small vibrations were observed. However, in the out-of-phase case, the tip was either attracted to the metal plate and repulsed by the incoming signal, or vice versa, which resulted in a large vibration. Thus, the phase could be described by the amplitude of the vibration, which was observable via the current. Moreover, applying a biased reference EM field \bar{E}_{ref} caused the motion of the CNT to become asymmetric when the center of the vibration was moved from its original equilibrium point o . This effect produced a component at the resonance frequency in the output current, and the phase could be observed by focusing on this component. Because this type of detector must be built at nanoscale, it contributes to the realization of nanoscale digital communications.

3. 2. Analytical Description of the Detector Output

For the designing of a demodulator with the proposed nanoscale detector, the output of the detector was analytically presented. Due to the quantum effects induced in the gap, a field emission current flowed between the anode and the CNT tip. Below, it is presented that the proposed detector enabled the current amplitude to describe the phase of the carrier signal; more precisely, the transmitted data were included in the components of the current at the resonance frequency f_r and double the resonance frequency $2f_r$. The analysis was twofold: the first step was the derivation of the position of the CNT tip (Sec. 3. 2. 1), followed by analysis of the field emission current based on the position (Sec. 3. 2. 2). This analysis also contributed to the derivation of the bit error rate (BER) performance, as discussed in Sec. 4.

3. 2. 1. CNT Tip Position

First, the position of the CNT tip was analytically derived. When the tip displacement was small relative to the CNT length, the motion of the tip could be described by the linear Euler–Bernoulli equation because the resonator was excited below the critical Duffing amplitude.⁽²⁸⁻³¹⁾ This motion could be described by the following second-order linear differential equation:

$$m_e \ddot{x} + \Gamma \dot{x} + k_0 x = F(t), \quad (1)$$

where $F(t)$ is the force applied to the tip. The other parameters in Eq. (1) are related to the CNT characteristics: m_e is the effective mass, L is the length, ρ is the radius, E_u is the Young's modulus, $k_0 = 3\pi E_u \rho^4 / 4L^3$ is the spring constant, $\Gamma = 2\pi m_e f_r / Q$ is the coefficient of the first-derivative term, Q is the quality factor, and $f_r = \sqrt{k_0 / m_e} / 2\pi$ is the resonance frequency. Note that the origin of the position (point o in Fig. 2(a)) was defined as the case without incoming EM and reference signals.

The key term in Eq. (1) is the force $F(t)$ which was induced by the EM field $E_d(t)$ around the tip, and by the amount of charge Q_{ext} on the tip. The EM field $E_d(t)$ is the combination of the incoming $E_{\text{in}}(t)$ and reference $E_{\text{ref}}(t)$ EM fields:

$$E_d(t) = E_{\text{in}}(t) - E_{\text{ref}}(t) = \tilde{E}_d \cos(2\pi f_c t + \alpha) - \bar{E}_{\text{ref}}, \quad (2)$$

where

$$\tilde{E}_d = \sqrt{E_b^2 + \tilde{E}_{\text{ref}}^2 - 2E_b \tilde{E}_{\text{ref}} \cos\theta_i} \quad (3)$$

and $\tan \alpha = E_b \sin\theta_i / (E_b \cos\theta_i - \tilde{E}_{\text{ref}})$. The EM field $E_d(t)$ depended on the transmitted data $\theta_i(t)$. The bias voltage V_{ext} , which was applied between the plate (anode) and the CNT, induced the charge around the tip. The analysis based on the image charge method gives the analytical expression for the amount of charge as $Q_{\text{ext}} = 4\pi\epsilon_0 L \rho V_{\text{ext}} \sum_{i=0}^{+\infty} \beta^i$, where $\beta = \rho / 2h_0$ and $\epsilon_0 = 8.854 \times 10^{-12}$ is the permittivity of vacuum.^(23,24,32)

The position of the CNT tip could be derived by solving Eq. (1) given $F(t) = Q_{\text{ext}} \tilde{E}_d(t)$. In the resonant mode, i.e., $f_c = f_r$, the solution could be simply given as

$$x(t) = \frac{Q_{\text{ext}} \tilde{E}_d}{2\pi f_r \Gamma} \cos(2\pi f_r t - \phi_r) - \frac{Q_{\text{ext}} \bar{E}_{\text{ref}}}{k_0}, \quad (4)$$

where $\phi_r = \pi/2 - \alpha = \pi/2 - \tan^{-1}(E_b \sin\theta_i / (E_b \cos\theta_i - \tilde{E}_{\text{ref}}))$. Note that in the above analysis, the tip vibration was assumed to be stabilized and was not in a transient state. In practice, every time the transmitted data d_i was changed, the vibration began in the transient mode

(Fig. 3). The position in this mode could be obtained through numerical simulation.

3. 2. 2. Field Emission Current

The mathematical expression for the field emission current is derived based on the results in Sec. 3. 2. 1. As discussed in Refs. (21), (23), and (24), the current can be described by Fowler–Nordheim tunneling:

$$I(t) = c_1 S (E_{\text{ext}}(h))^2 e^{-c_2/E_{\text{ext}}(h)}, \quad (5)$$

where h is the distance from the tip to the anode, $S = \pi\rho^2$ is the area where the electron emits, and $E_{\text{ext}}(h)$ is the EM field between the CNT tip and the anode. The two constants $c_1 = 3.4 \times 10^{-5} \text{ A/V}^2$ and $c_2 = 7.0 \times 10^{10} \text{ V/m}$ are given in Ref. (21). Because of the tip vibration, the distance included the variation term $\Delta h(t)$, i.e., $h(t) = h_0 + \Delta h(t)$. For small

variations, the Taylor expansion of Eq. (5) around $h(t) = h_0$, excluding terms higher than second order yields

$$I(t) = I_0 + \Delta I(t), \quad (6)$$

where

$$\Delta I(t) = \kappa I_0 x^2(t) \quad (7)$$

and $\kappa = (2 + c_2/E_{\text{ext}}(h_0))(\partial E_{\text{ext}}/\partial h)_{h=h_0}/2LE_{\text{ext}}(h_0)$ and $I_0 = c_1 S E_{\text{ext}}^2(h_0) e^{-c_2/E_{\text{ext}}(h_0)}$. Substituting Eq. (4) into Eq. (7) gave the following detailed expression of the variation term $\Delta I(t)$:

$$\begin{aligned} \Delta I(t) = & -\frac{\xi Q \bar{E}_d^2}{2} \cos(4\pi f_r t + 2\alpha) \\ & + 2\xi \bar{E}_d \bar{E}_{\text{ref}} \sin(2\pi f_r t + \alpha) \\ & + \frac{\xi k_0 \bar{E}_{\text{ref}}^2}{Q} + \frac{\xi Q \bar{E}_d^2}{2} \end{aligned} \quad (8)$$

where

$$\xi = \kappa I_0 Q Q_{\text{ext}}^2 / k_0^2 \quad (9)$$

is the key parameter that described the influence of the nanoscale reception and detection. This influence will be numerically discussed in Sec. 5. 2.

Unlike the system in Ref. (21), an additional term at f_r term appeared in Eq. (8). When the biased reference EM field from the plate was applied, the equilibrium point (point o in Fig. 2(a)) was shifted to the plate. This shift was the source of asymmetric vibration of the tip, and the distance $h(t)$ between the tip and the anode varied at rates of f_r and $2f_r$. Thus, the components of the current at both frequencies could be used to describe the data. The next section discusses how the transmitted data can be estimated by focusing on these frequencies.

The current in the original system⁽²¹⁾ was described by Eq. (8) with $\bar{E}_{\text{ref}} = 0$ and $\bar{E}_{\text{ref}} = 0$. In this case, we have

$$\Delta I(t) = \xi Q E_0^2 (\cos(4\pi f_r t + 2\theta_0) - 1)/2. \quad (10)$$

This equation indicates that the current does not vary with the transmitted data θ_i ; that is, the original system⁽²¹⁾ has been analytically shown to not give phase information in the output.

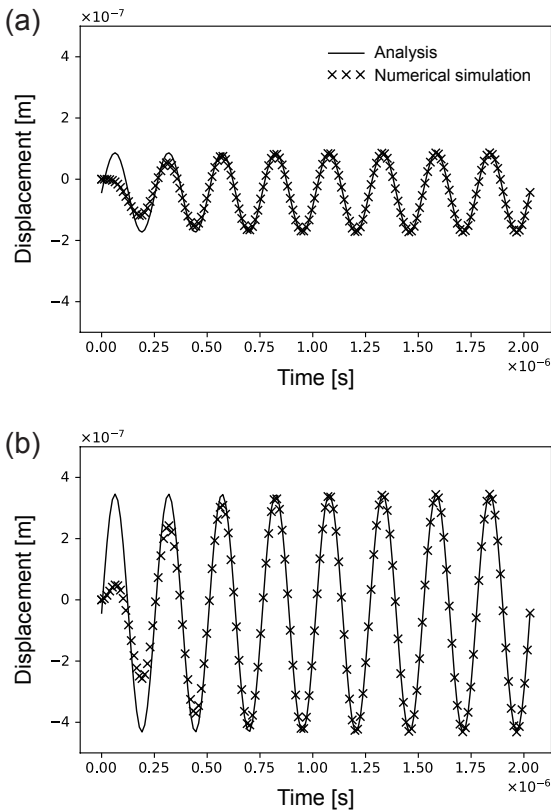


Fig. 3 (a) Examples of trajectories of the CNT tip at $\theta_i = 0$. (b) Examples of trajectories of the CNT tip at $\theta_i = \pi$.

4. Demodulator Design for the System with the Proposed Nanoscale Phase Detector

The design framework for the demodulator was based on the proposed nanoscale phase detector. The transmitted data could be estimated from the output, i.e., the field emission current $I(t)$. In this study, a simple correlator is used to describe the fundamental characteristics in the communication system, including the BER. The performance gain is analytically discussed in terms of the BER.

With the use of a traditional correlator, the field emission current is simply correlated with the carrier signal for one-bit duration T_b , and the decision statistic is obtained. The data is estimated by taking hard decision of the statistic. A schematic of this proposed demodulator is shown in **Fig. 4**. When a carrier signal with a frequency of f_r was used, the correlator outputs the following decision statistic:

$$\begin{aligned} r_{f_r} &= \frac{1}{T_b} \int_{(i-1)T_b}^{iT_b} \{I(t) + n(t)\} \cos(2\pi f_r t) dt \\ &= -\xi \bar{E}_{\text{ref}} \sqrt{\varepsilon_b} d_i \sin \theta_0 + n_i \end{aligned} \quad (11)$$

Here, the term $\varepsilon_b = E_b^2 T_b$ denotes the signal power per bit. The estimated data was obtained as $\hat{d}_i = \text{sgn}(r_{f_r}[i])$, where $\text{sgn}(\cdot)$ extracts the sign.

The BER performance was derived based on the analytical expression of the statistic Eq. (11). This equation indicated that the distance between the received signal points for BPSK signaling was $\Lambda_{f_r} = |r_{f_r}[i]_{d_i=+1} - r_{f_r}[i]_{d_i=-1}| = \sqrt{\varepsilon_b} |2\xi \bar{E}_{\text{ref}} \sin \theta_0|$. Since the noise was white Gaussian noise, the BER was obtained as

$$\begin{aligned} \text{BER}_{f_r} &= \Psi \left(\sqrt{\Lambda_{f_r}^2 / 2N_0} \right) \\ &= \Psi \left(|\xi \bar{E}_{\text{ref}} \sin \theta_0| \sqrt{\varepsilon_b / N_0} \right), \end{aligned} \quad (12)$$

where $\Psi(z) = \left(\int_z^{+\infty} e^{-u^2/2} du \right) / \sqrt{2\pi}$ is the Q-function representing the tail probability of the standard Gaussian distribution, $e^{-u^2/2}$. In the case with a frequency of $2f_r$, the BER could be obtained in a similar manner with the following correlator output:

$$r_{2f_r} = \frac{1}{2} \xi Q \tilde{E}_{\text{ref}} \sqrt{\varepsilon_b} d_i \cos \theta_0 + n_i. \quad (13)$$

The above analysis indicates that the BER performance with the simple correlator should be worse than that of the traditional BPSK receiver; from Eqs. (11) and (13), the signal-to-noise power ratio per bit, which is an important performance measures, is multiplied by the coefficients, $|\xi \bar{E}_{\text{ref}} \sin \theta_0|$ for f_r , and $|(\xi Q \tilde{E}_{\text{ref}} \cos \theta_0)/2|$ for $2f_r$. As discussed in the next section, these coefficients are significantly smaller than 1.0, showing that reduction of the signal power results in the deterioration of the BER.

5. Numerical Examples on the Proposed Nanoscale Phase Detector

Numerical examples are presented to discuss the basic characteristics of the proposed nanoscale phase detector and the communication performance with the demodulators.

The values of the parameters used in this section are given as follows: $m_e = 0.24 \times 10^{-17}$ kg, $L = 1.0 \mu\text{m}$, $\rho = 5.0$ nm, $E_u = 1.0 \times 10^{12}$ Pa, $Q = 3$, $h_0 = 20.0$ nm, $d_0 = 1.0 \mu\text{m}$, $f_c = 3.9$ MHz, $\tilde{E}_{\text{in}} = 1.0 \times 10^6$ V/m, $\tilde{E}_{\text{ref}} = 2.0 \times 10^6$ V/m, $\bar{E}_{\text{ref}} = 1.0 \times 10^6$ V/m. Since the aim of this study was to provide a method of miniaturizing the front end of the receiver, the key parameters that determine device size, i.e., the CNT length and the distance between the plates, were set to be on nanoscale. The values of the other parameters were set based on Ref. (21). Under this condition, the resonance frequency f_r was approximately 4.0 MHz, which was equal to the carrier frequency f_c .

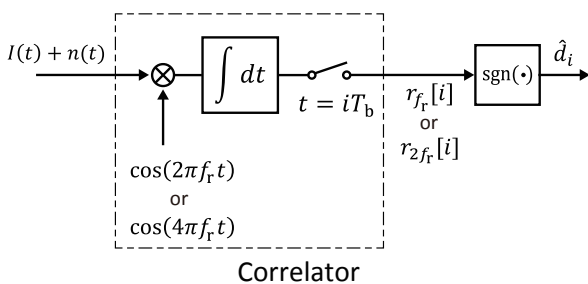


Fig. 4 Schematic diagram of the demodulator (correlator).

5. 1. Examples of CNT Tip Vibration

Figure 4(a) shows the trajectory of the CNT tip in the proposed phase detector. To obtain the results in this figure, the parameters related to the EM field were set to $E_b = 1.0 \times 10^6$ V/m, $\tilde{E}_{ref} = 2.0 \times 10^6$ V/m, $\bar{E}_{ref} = 1.0 \times 10^6$ V/m, $Q = 3.0$, and $V_{ext} = 100$ V. The curves in Fig. 4(a) were obtained from Eq. (4). Except in the transient state, the theoretical curves were found to be in good agreement with the numerical results which were obtained by solving Eq. (1) with the initial position set to point o . This result confirms validity of the analysis presented in Sec. 3. 2. 1 is valid.

Based on the discussion in Sec. 4, the amplitude of the vibration should depend on the phase θ_i . This behavior was clearly confirmed in Fig. 4(a). In the case of $\theta_i = 0$, the two EM waves simultaneously applied repulsive or attractive force to the CNT tip, resulting in small vibrations. In contrast, in the case of $\theta_i = \pi$, large vibrations are observed as shown in Fig. 4(b). When a repulsive force was applied by the incoming EM signal $E_{in}(t)$, the force attracted the tip, and the reference EM simultaneously pulled the tip. As a result of this electro-magnetic interaction between the two waves on the tip, the proposed nanoscale detector converted the phase θ_i into the amplitude of the vibration.

The observed discrepancy in the transient state provides insight into the design of the communication and device parameters. In the proposed detector, the tip vibration should track the phase θ_i . However, because of the inertial effect, the CNT tip could not quickly respond to changes in the phase. The amount of time required for the tip to show a full response (i.e., time to achieve a stable state) was estimated in terms of the signal period and was found to be roughly equal to Q . In other words, the phase must be kept constant for at least in Q periods, that is, $Q/f_c < T_b$.

5. 2. Examples of BER

The discussion in this section focuses on the BER performance. The first example system used simple correlators with the frequencies f_r and $2f_r$, and the results of which are depicted in Fig. 5. The parameters used to obtain these results were $\tilde{E}_{ref} = 4.0 \times 10^2$ V/m, $\bar{E}_{ref} = 1.0 \times 10^7$ V/m, and $V_{ext} = 500$ V. For reference, the well-known theoretical BPSK performance, $\Psi(\sqrt{2\varepsilon_b/N_0})$, is also plotted

in this figure. To enable the clear observation of the dependence of the BER on θ_0 , the quality factor was changed to $Q = 8.0 \times 10^4$.

A key point from this Fig. 5 is that the performance strongly depends on the phase offset, θ_0 . For example, in the case of f_r , the proposed system successfully received the data with a difference of $\theta_0 = \pi/2$. However, in the case of $\theta_0 = \{0, \pi\}$, $BER_{f_r} = 0.5$ for any ε_b/N_0 , indicating that the receiver did not obtain any transmitted data. In fact, this point was analytically predicted; from Eq. (12), where BER is a function of $\sin \theta_0$. When the phase difference satisfied the condition in Eq. (12): $\sin \theta_0 = 0$, and the proposed method was no longer valid. The optimal phase offset, which realizes a low BER in terms of the phase difference, could be derived by maximizing the distance Λ_{f_r} of the signal points as

$$\hat{\theta}_0 = \arg \max_{\theta_0} \Lambda_{f_r} = \arg \max_{\theta_0} |\sin \theta_0|. \quad (14)$$

Note that $0 \leq \theta_0 \leq \pi$ was focused.

Although the optimization of the phase difference was effective, the BER required further improvement. Figure 5 shows that the BER of the BPSK theory was not achieved in the proposed system. This disadvantage is the price of achieving reception and phase detection at nanoscale. In a traditional receiver, the antenna size is on the order of one signal wavelength; thus, the obtained signal power is sufficiently large to keep the BER low. The proposed detector realizes

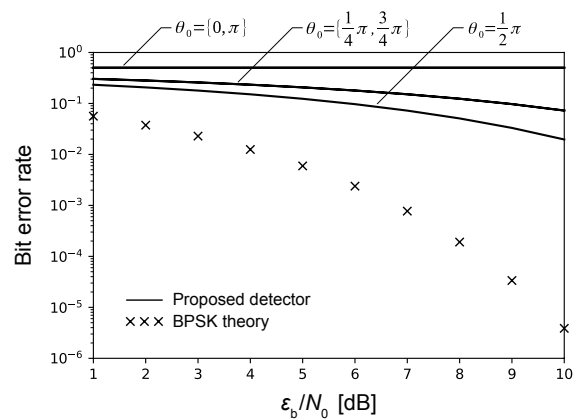


Fig. 5 BER performance of the system with the proposed nanoscale phase detector and the simple correlators for f_r .

reception/detection at nanoscale but in exchange reduces the signal power. Indeed, the present analytical results calculated using Eqs. (12) and (13) showed that the signal power is decreased by a factor of ξ . For example, in the case of Fig. 5, $\xi = 6.52 \times 10^{-8}$ indicates a severe reduction in power. This parameter, which is given in Eq. (9), is key in the sense that it describes the nanoscale effects of the system. Therefore, the device parameters should be properly designed to realize a sufficiently large value of ξ .

6. Noise-enhanced Field Emission Current

6.1. Concept and Numerical Example of the Enhancement

To enhance the signal in the demodulation, the fundamental framework of Fowler–Nordheim tunneling, which is described in Eq. (5), is focused. Because this current has nonlinear behavior of exponential form, SR should be observed by the addition of noise. In this method, the bias voltage V_{ext} may contain the noise. However, simply considering the noise does not achieve the amplification of the current. We found that an additional method in signal processing, time averaging of the noisy current, is required.

Simple white Gaussian noise was focused as the noise component of the bias voltage. The mean of the noise was assumed to be zero, and the variance was σ^2 . In this case, the voltage became a stochastic process $n_V(t)$ whose probability density followed that of white Gaussian noise with a mean of V_{ext} and a variance of σ^2 . The noisy field emission current, which is denoted as $\tilde{I}(t)$, was obtained by Eq. (5) in which V_{ext} was replaced with $n_V(t)$. **Figure 6** gives an example of the field emission current excited by a noisy bias voltage. This curve was obtained under the following conditions: $V_{\text{ext}} = 50.0 \text{ V}$, $\sigma = 1.0 \text{ V}$, $c_1 = 3.2 \times 10^{-7}$, $c_2 = 7.18 \times 10^{10}$, $\rho = 10.0 \text{ nm}$, and $h_0 = 40.0 \text{ nm}$. Without the noise, the current would have a constant value of $I = 6.20 \times 10^{-16} \text{ A}$. With noise, $\tilde{I}(t)$ showed stochastic behavior; however, the noisy current was simply a weak signal buried in the noise.

To achieve the noise-induced amplification, the time-averaging of the noisy current, $\bar{I} = \left(\int_0^{T_{\text{av}}} \tilde{I}(t) dt \right) / T_{\text{av}}$, was introduced. Here, T_{av} is the time interval over which the current is averaged.

As shown in Fig. 6, the average current was amplified to $\bar{I} = 7.34 \times 10^{-16} \text{ A}$. To investigate the magnitude of this effect, the current enhancement $\gamma = \bar{I} - I$ was evaluated under different conditions, as shown in **Fig. 7**. As the mean value of the bias voltage, V_{ext} , was increased, the averaged current was strongly amplified. Moreover, as the noise variance increased, the current enhancement also increased; that is, there is no maximum limit to the enhancement was observed. This dependence on the noise variance is not trivial because, in traditional SR systems, the system response reaches a peak at a certain noise intensity.^(25,27) To justify this behavior, the enhancement mechanism is presented in the next section.

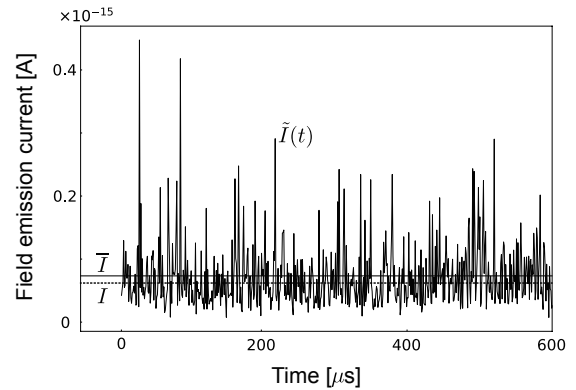


Fig. 6 Example of the noise enhancement of the field emission current.

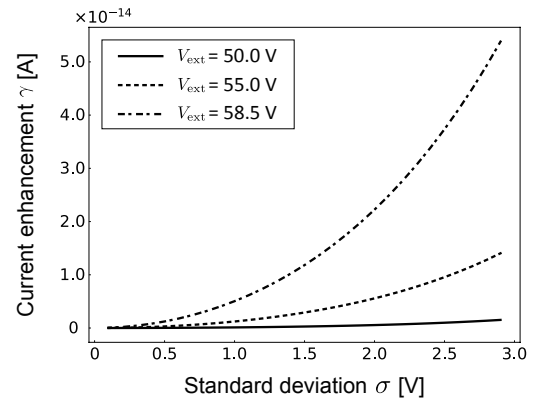


Fig. 7 The current enhancement γ obtained as the result of SR.

6.2. Numerical Examples

In the proposed method, current enhancement was achieved as the result of probability density modulation of the noisy field emission current. Through the examples depicted in Fig. 8, this section will explain the core concept of the proposed method.

Figure 8(a) shows the probability density of the noisy bias voltage $n_V(t)$. As described in the previous section, this signal follows a Gaussian distribution with a mean of V_{ext} and a variance of σ^2 . This stochastic voltage is applied to the anode. Because of the exponential shape of the nonlinear field emission current response, which is shown in Fig. 8(b), the resulting probability density of the noisy field emission current is heavy-tailed distribution, as shown in Fig. 8(c). The heavy-tailed portion of the distribution contributes to the amplification of the time-averaged current \bar{I} , indicated by the solid line in Figs. 8(b) and (c). The mean of the original distribution shown in Fig. 8(a) is $V_{\text{ext}} = 50.0$ V, and the corresponding field emission current is indicated by the dotted line in Figs. 8(b) and (c). The time-averaged current \bar{I} is larger than the current corresponding to the mean voltage, and

the difference between the two describes the current enhancement γ .

Based on the above discussion, the reason that the curves in Fig. 7 do not have a limiting value can be explained. As the variance increases, the tail of the heavy-tailed distribution of the field emission current increases without limit. Thus, the time-averaged current \bar{I} is proportional to the variance. However, in practical systems, actual devices have a limit to the range of input voltages they can receive. Therefore, the voltage of a noisy signal with a large variance would often exceed the input voltage limit, and the resulting probability density would thus be clipped in the region of large current. In this situation, the time-averaged current would converge to a certain value, representing the limit to achievable amplification.

7. Conclusion

To achieve to digitally receive and detect phase-modulated signals in nanoscale, a nanoscale phase detector was proposed in this study. Two important functions for communications: reception and detection of signals were realized at the nanoscale, by exploiting the mechanical vibration of a CNT tip, which is controlled by the reference EM field from a metal plate. Our theoretical analysis demonstrated the possibility of detection; however, the nanoscale reception unfortunately reduces the received signal power. For this problem, a counter-method of the current enhancement was introduced; the time averaging of the noisy field emission current served to amplify the received signal. The effectiveness of the method was numerically demonstrated. This point was supported by analytical description of the mechanism of the enhancement.

Acknowledgments

This study was partly supported by JSPS KAKENHI grant number JP17K14690.

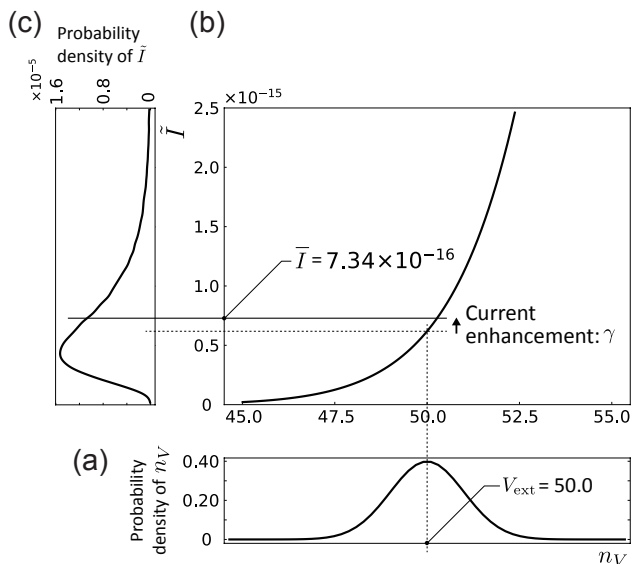


Fig. 8 Mechanism of the enhancement of the field emission current by noise. (a) probability density of the noisy bias voltage, $n_V(t)$, (b) response curve of the field emission current for the noisy bias voltage, and (c) probability density of the noisy current, \tilde{I} .

References

- (1) Gardašević, G., Veletić, M., Maletić, N., Vasiljević, D., Radusinović, I., Tomović, S. and Radonjić, M., “The IoT Architectural Framework, Design Issues and Application Domains”, *Wireless Pers. Commun.*, Vol. 92, No. 1 (2017), pp. 127-148.
- (2) Kahn, J. M., Katz, R. H. and Pister, K. S. J., “Next Century Challenges: Mobile Networking for ‘Smart Dust’”, *Proc. 5th Annu. ACM/IEEE Int. Conf. Mobile Comput. Netw.* (1999), pp. 271-278, IEEE.
- (3) Warneke, B. A., Scott, M. D., Leibowitz, B. S., Zhou, L., Bellew, C. L., Chediak, J. A., Kahn, J. M., Boser, B. E. and Pister, K. S. J., “An Autonomous 16 mm³ Solar-powered Node for Distributed Wireless Sensor Networks”, *Proc. IEEE Sensors*, Vol. 2 (2002), pp. 1510-1515, IEEE.
- (4) Akyildiz, I. F., Jornet, J. M. and Pierobon, M., “Nanonetworks: A New Frontier in Communications”, *Commun. ACM*, Vol. 54, No. 11 (2011), pp. 84-89.
- (5) Atakan, B. and Akan, O. B., “Carbon Nanotube-based Nanoscale Ad Hoc Networks”, *IEEE Commun. Mag.*, Vol. 48, No. 6 (2010), pp. 129-135.
- (6) Stutzman, W. L. and Thiele, G. A., *Antenna Theory and Design* (1981), 598p., Wiley.
- (7) Jornet, J. M. and Akyildiz, I. F., “Joint Energy Harvesting and Communication Analysis for Perpetual Wireless Nanosensor Networks in the Terahertz Band”, *IEEE Trans. Nanotechnol.*, Vol. 11, No. 3 (2012), pp. 570-580.
- (8) Jornet, J. M. and Akyildiz, I. F., “Graphene-based Plasmonic Nano-antenna for Terahertz Band Communication in Nanonetworks”, *IEEE J. Sel. Area Commun.*, Vol. 31, No. 12 (2013), pp. 685-694.
- (9) Sugiura, S. and Iizuka, H., “Deep-subwavelength MIMO Using Graphene-based Nanoscale Communication Channel”, *IEEE Access*, Vol. 2 (2014), pp. 1240-1247.
- (10) Craighead, H. G., “Nanoelectromechanical Systems”, *Science*, Vol. 290, No. 5496 (2000), p. 1532-1535.
- (11) Ayari, A., Vincent, P., Perisanu, S., Choueib, M., Gouttenoire, V., Bechelany, M., Cornu, D. and Purcell, S. T., “Self-oscillations in Field Emission Nanowire Mechanical Resonators: A Nanometric DC-AC Conversion”, *Nano Lett.*, Vol. 7, No. 8 (2007), pp. 2252-2257.
- (12) Moser, J., Eichler, A., Güttinger, J., Dykman, M. I. and Bachtold, A., “Nanotube Mechanical Resonators with Quality Factors of up to 5 Million”, *Nat. Nanotechnol.*, Vol. 9 (2014), pp.1007-1011.
- (13) Eom, K., Park, H. S., Yoon, D. S. and Kwon, T., “Nanomechanical Resonators and Their Applications in Biological/Chemical Detection: Nanomechanics Principles”, *Phys. Rep.*, Vol. 503, No. 4-5 (2011), pp. 115-163.
- (14) Kosaka, P. M., Pini, V., Ruz, J. J., da Silva, R. A., González, M. U., Ramos, D., Calleja, M. and Tamayo, J., “Detection of Cancer Biomarkers in Serum Using a Hybrid Mechanical and Optoplasmonic Nanosensor”, *Nat. Nanotechnol.*, Vol. 9, No. 12 (2014), pp. 1047-1053.
- (15) Kuo, C. Y., Chan, C. L., Gau, C., Liu, C.-W., Shiau, S. H. and Ting, J.-H., “Nano Temperature Sensor Using Selective Lateral Growth of Carbon Nanotube between Electrodes”, *IEEE Trans. Nanotechnol.*, Vol. 6, No. 1 (2007), pp. 63-69.
- (16) Malvar, O., Ruz, J. J., Kosaka, P. M., Dominguez, C. M., Gil-Santos, E., Calleja, M. and Tamayo, J., “Mass and Stiffness Spectrometry of Nanoparticles and Whole Intact Bacteria by Multimode Nanomechanical Resonators”, *Nat. Commun.*, Vol. 7 (2016), 13452.
- (17) Weber, P., Güttinger, J., Noury, A., Vergara-Cruz, J. and Bachtold, A., “Force Sensitivity of Multilayer Graphene Optomechanical Devices”, *Nat. Commun.*, Vol. 7 (2016), 12496.
- (18) Souayeh, S. and Kacem, N., “Computational Models for Large Amplitude Nonlinear Vibrations of Electrostatically Actuated Carbon Nanotube-based Mass Sensors”, *Sens. Actuators, A*, Vol. 208 (2014), pp. 10-20.
- (19) Eichler, A., Moser, J., Chaste, J., Zdrojek, M., Wilson-Rae, I. and Bachtold, A., “Nonlinear Damping in Mechanical Resonators Made from Carbon Nanotubes and Graphene”, *Nat. Nanotechnol.*, Vol. 6, No. 6 (2011), pp. 339-342.
- (20) Ouakad, H. M. and Younis, M. I., “Nonlinear Dynamics of Electrically Actuated Carbon Nanotube Resonators”, *J. Comput. Nonlinear Dyn.*, Vol. 5, No. 1 (2009), 011009.
- (21) Jensen, K., Weldon, J., Garcia, H. and Zettl, A., “Nanotube Radio”, *Nano Lett.*, Vol. 7, No. 11 (2007), pp. 3508-3511.
- (22) Vincent, P., Poncharal, P., Barois, T., Perisanu, S., Gouttenoire, V., Frachon, H., Lazarus, A., de Langre, E., Minoux, E., Charles, M., Ziaei, A., Guillot, D., Choueib, M., Ayari, A. and Purcell, S. T., “Performance of Field-emitting Resonating Carbon Nanotubes as Radio-frequency Demodulators”, *Phys. Rev. B*, Vol. 83, No. 15 (2011), 155446.
- (23) Tanaka, H., Ohno, Y. and Tadokoro, Y., “Angular Sensitivity of VHF-band CNT Antenna”, *IEEE Trans. Nanotechnol.*, Vol. 14, No. 6 (2015), pp. 1112-1116.
- (24) Tanaka, H., Ohno, Y. and Tadokoro, Y., “Adaptive Control of Angular Sensitivity for VHF-band Nano-antenna Using CNT Mechanical Resonator”, *IEEE Trans. Molecular, Biological and Multi-scale Commun.*, Vol. 3, No. 1 (2017), pp. 24-32.
- (25) Gammaitoni, L., Hänggi, P., Jung, P. and Marchesoni, F., “Stochastic Resonance”, *Rev. Mod. Phys.*, Vol. 70, No. 1 (1998), pp. 223-287.

- (26) Godivier, X., Rojas-Varela, J. and Chapeau-Blondeau, F., "Noise-assisted Signal Transmission via Stochastic Resonance in a Diode Nonlinearity", *Electron. Lett.*, Vol. 33, No. 20 (1997), pp. 1666-1668.
- (27) Kasai, S. and Asai, T., "Stochastic Resonance in Schottky Wrap Gate-controlled GaAs Nanowire Field-effect Transistors and Their Networks", *Appl. Phys. Express*, Vol. 1, No. 8 (2008), 083001.
- (28) Cleland, A. N., *Foundations of Nanomechanics: From Solid State Theory to Device Applications* (2003), 436p., Springer.
- (29) Juillard, J., Bonnoit, A., Avignon, E., Hentz, S., Kacem, N. and Colinet, E., "From MEMS to NEMS: Closed-loop Actuation of Resonant Beams beyond the Critical Duffing Amplitude", *Proc. 2008 IEEE Sensors* (2008), pp. 510-513, IEEE.
- (30) Kacem, N., Baguet, S., Hentz, S. and Dufour, R., "Nonlinear Phenomena in Nanomechanical Resonators: Mechanical Behaviors and Physical Limitations", *Mech. Ind.*, Vol. 11, No. 6 (2010), pp. 521-529.
- (31) Kacem, N., Baguet, S., Duraffourg, L., Jourdan, G., Dufour, R. and Hentz, S., "Overcoming Limitations of Nanomechanical Resonators with Simultaneous Resonances", *Appl. Phys. Lett.*, Vol. 107, No. 7 (2015), 073105.
- (32) Smythe, W. R., *Static and Dynamic Electricity* (1950), 616p., McGraw-Hill.

Figs. 1-5

Reprinted from *IEEE Trans. Nanotechnol.*, Vol. 17, No. 1 (2018), pp. 84-92, Tadokoro, Y., Ohno, Y., and Tanaka, H., Detection of Digitally Phase-modulated Signals Utilizing Mechanical Vibration of CNT Cantilever, © 2017 IEEE, with permission from IEEE.

Figs. 6-8

Reprinted from *Electron. Lett.*, Vol. 54, No. 12 (2018), pp. 770-772, Tadokoro, Y., Funayama, K., and Tanaka, H., Noise-enhanced Field Emission Current from a Carbon Nanotube Cantilever, © 2018 The Institution of Engineering and Technology, with permission from The Institution of Engineering and Technology.

Yukihiro Tadokoro

Research Fields:

- Nonlinear Signal Processing Exploiting Noise
- Nanomechanical Systems for Signal Processing
- Wireless Communications

Academic Degree: Dr.Eng.

Academic Societies:

- IEEE Nanotechnology Council
- IEICE NOLTA Society

Award:

- Telecom System Technology Award, The Telecommunication Advancement Foundation, 2017



Hiroya Tanaka

Research Fields:

- Nonlinear Signal Processing Exploiting Noise
- Nanomechanical Systems for Signal Processing
- Wireless Communications
- Applied Radio Instrumentation and Measurements

Academic Degree: Dr.Eng.

Academic Society:

- IEEE Microwave Theory and Techniques Society

Award:

- Telecom System Technology Award, The Telecommunication Advancement Foundation, 2017



Keita Funayama

Research Fields:

- Nanomechanical Systems for Signal Processing
- Nano-electronical Devices



Yutaka Ohno*

Research Field:

- Low-dimensional Materials and Their Electronics Applications

Academic Degree: Ph.D.

Academic Societies:

- The Japan Society of Applied Physics
- The Institute of Electronics, Information and Communication Engineers
- The Fullerenes and Nanotubes Research Society
- American Chemical Society
- Material Research Society

Awards:

- Lee Hsun Research Award, Institute of Metal Research, Chinese Academy of Sciences, 2019
- Academic Award, The NAGAI Foundation for Science & Technology, 2016
- APEX/JJAP Editorial Contribution Award, The Japan Society of Applied Physics, 2012



*Nagoya University